International Journal of Architectural, Civil and Construction Sciences
ISSN: 2415-1734
Vol:6, No:2, 2012

The Effect of Frame Geometry on the Seismic Response of Self-Centering Concentrically-Braced Frames

David A. Roke and M. R. Hasan

Abstract**—**Conventional concentrically-braced frame (CBF) systems have limited drift capacity before brace buckling and related damage leads to deterioration in strength and stiffness. Self-centering concentrically-braced frame (SC-CBF) systems have been developed to increase drift capacity prior to initiation of damage and minimize residual drift. SC-CBFs differ from conventional CBFs in that the SC-CBF columns are designed to uplift from the foundation at a specified level of lateral loading, initiating a rigid-body rotation (rocking) of the frame. Vertically-aligned post-tensioning bars resist uplift and provide a restoring force to return the SC-CBF columns to the foundation (self-centering the system). This paper presents a parametric study of different prototype buildings using SC-CBFs. The bay widths of the SC-CBFs have been varied in these buildings to study different geometries. Nonlinear numerical analyses of the different SC-CBFs are presented to illustrate the effect of frame geometry on the behavior and dynamic response of the SC-CBF system.

Keywords**—**Earthquake resistant structures, nonlinear analysis, seismic analysis, self-centering structural systems.

I. Introduction

STEEL concentrically-braced frame (CBF) systems are stiff and economical earthquake-resistant steel frame systems that often have limited system ductility capacity before structural damage initiates. Under the design basis earthquake, CBF systems are expected to undergo drift demands that cause the braces to buckle or yield, leading to residual drift after the earthquake. Ductility capacity can be increased through the use of buckling-restrained braces [1]-[2]; however, buckling-restrained braced frame systems may exhibit significant residual drift after an earthquake [2]. Self-centering concentrically-braced frame (SC-CBF) systems have been developed to maintain the advantages of conventional CBF systems (i.e., economy and stiffness) while increasing the lateral drift capacity prior to the initiation of structural damage and decreasing the residual lateral drift [3].

SC-CBF systems that permit column uplift without restraint from the adjacent gravity load carrying beams have been developed [4]. Lateral forces are transmitted into the SC-CBF through lateral-load bearings that develop friction forces that help resist uplift of the SC-CBF columns.

David A. Roke is an Assistant Professor at the Department of Civil Engineering, The University of Akron, Akron, OH 44325 USA (email: *roke@uakron.edu).*

M. R. Hasan is a Graduate Research Assistant at the Department of Civil Engineering, The University of Akron, Akron, OH 44325 USA (email: *mh94@zips.uakron.edu).*

Previous research identified overturning moment as the main strength parameter for the SC-CBF structures and introduced a design parameter η that quantifies the overturning moment resistance provided by the friction energy dissipation elements [5]. η is a function of frame geometry; in this study, frame geometry is varied to determine the effect of the variation of η on the seismic response of SC-CBF systems.

This paper presents a parametric study of the response of SC-CBFs with different frame geometries (different values of η). SC-CBF systems with similar floor plans but different frame bay widths were designed and studied. Static and dynamic nonlinear numerical analysis results are presented for each frame design to show the effect that changing the value of η has on the performance and behavior of the SC-CBF system.

II. System Behavior

The SC-CBF system considered in this study is shown schematically in Fig. 1(a). The beams, columns, and braces of the SC-CBF are in a conventional arrangement; however, details at the SC-CBF column bases permit decompression and uplift, enabling rocking of the SC-CBF. Two sets of columns are indicated in Fig. 1(a): SC-CBF columns, which are permitted to uplift from the foundation as shown in Fig. 1(b), and the adjacent gravity columns, which do not uplift. At each floor level, lateral-load bearings are designed to transmit lateral inertia forces from the adjacent gravity columns (which are connected to the floor diaphragms) into the SC-CBF (which is not connected to the floor diaphragms). These lateral-load bearings allow relative vertical displacements between the SC-CBF columns and the adjacent gravity columns. Self-weight of the SC-CBF members, friction at the lateral-load bearings, and post-tensioning (PT) forces in the PT bars resist column uplift and provide a restoring force after uplift occurs. The SC-CBF includes a distribution strut to transfer the PT bar force to the braces.

Under low levels of lateral force, the structure deforms elastically, similar to the response of a conventional CBF. Overturning moment from the lateral forces causes a reduction in the compression force in one SC-CBF column; under higher levels of lateral force, this effect overcomes the initial compression in that SC-CBF column. This causes the SC-CBF column to decompress and uplift, and rocking behavior initiates as shown in Fig. 1(b). The rocking behavior consists

of two drift components: (1) elastic deformation that is similar to that of a conventional CBF, and (2) rigid-body rotation about the base of the compression column.

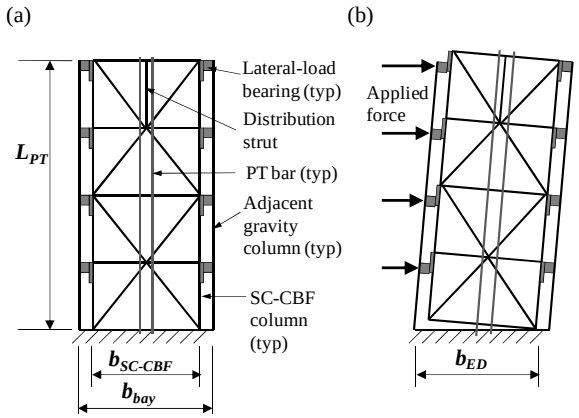

Fig. 1 SC-CBF concept: (a) configuration; (b) rocking behavior.

A free-body diagram of the SC-CBF at column decompression is shown in Fig. 2(a). The applied overturning moment (from the lateral forces F_i) is equal to the overturning moment at decompression (OM_D) and is resisted by the initial PT bar force (PT_0), the self-weight of the SC-CBF members (W), and the friction forces at the lateral-load bearings at each floor (F_{EDi}). By definition, at column decompression, only one SC-CBF column transmits vertical loads to the foundation. Further increases in applied overturning moment will cause the SC-CBF column with zero vertical reaction to uplift from its base and will elongate the PT bars.

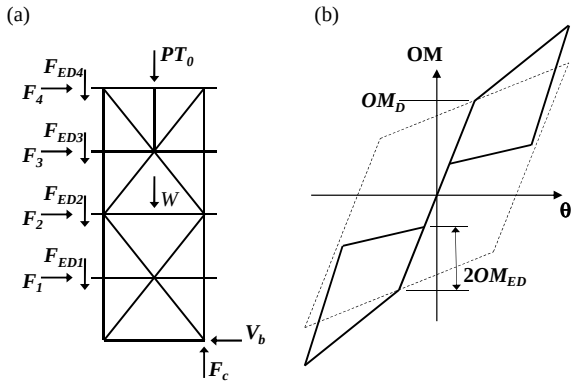

Fig. 2 SC-CBF behavior: (a) free body diagram at column decompression; (b) hysteretic response.

Elongation of the PT bars increases the PT bar force, providing a positive stiffness to the post-decompression lateral force-lateral drift behavior, as shown in Fig. 2(b). Rocking and the associated rigid-body rotation dominate the roof drift response after column decompression because the post-decompression stiffness is much less than the elastic stiffness of the SC-CBF. Therefore, the increases in elastic deformations and internal forces in the SC-CBF members are limited by the rocking behavior, resulting in a larger lateral drift capacity prior to the initiation of structural damage.

Cyclic loading of an SC-CBF results in the hysteretic behavior shown in Fig. 2(b). The dashed lines indicate the hysteretic behavior of a bilinear elastic system with the same strength (OM_D) under cyclic loading to the same peak roof drift. The solid lines indicate the hysteretic behavior of an SC-CBF with friction-based energy dissipation. Note that the friction at the lateral-load bearings increases the post-decompression stiffness of the SC-CBF with respect to that of the bilinear elastic stiffness. The flag-shaped hysteresis exhibited by the SC-CBF is characteristic of self-centering structural systems. The width of the hysteresis loop is equal to twice the overturning moment resisted by the friction in the lateral-load bearings, OM_{ED}, which is determined as follows [5]:

$$OM_{ED} = \sum_{i=1}^{4} F_{ED,i} \cdot b_{ED} = \mu \cdot \sum_{i=1}^{4} F_i \cdot b_{ED} = \mu \cdot V_b \cdot b_{ED} \qquad (1)$$

where μ is the coefficient of friction at the lateral load bearings between the SC-CBF columns and the adjacent gravity columns; b_{ED} is the distance between the SC-CBF column and the adjacent gravity column of the opposite side (as shown in Fig. 1(b)); and V_b is the base shear, which is equal to the ratio of the applied overturning moment (OM) to the effective height of the structure (h^*). Therefore, (1) can be rewritten as [5]:

$$OM_{ED} = \mu \cdot \frac{OM}{h^*} \cdot b_{ED} = \mu \cdot \frac{b_{ED}}{h^*} \cdot OM = \eta \cdot OM \qquad (2)$$

Here η is a dimensionless design parameter relating the overturning moment resisted by the friction in the lateral load bearings to the applied overturning moment. η is a function of frame geometry and friction properties at the lateral load bearings.

III. Prototype Structures

Three prototype structures were designed using SC-CBFs with friction-based energy dissipation as the lateral force resisting system. The prototype structures are four-story office buildings designed for a site with stiff soil in Van Nuys, CA. The prototype structures have equal floor areas and identical story heights. Building dimensions are given in Fig. 3(a). The coefficient of friction (μ) at the lateral load bearings between the SC-CBF columns and the adjacent gravity columns is assumed to be equal to 0.45 for all three prototype structures. Therefore, to vary the parameter η, the typical floor plans for the prototype structures are different, as shown in Fig. 3. Each prototype structure has four SC-CBFs in each direction, but the bay widths of the SC-CBFs are varied. The SC-CBFs designed for the prototype structure floor plans shown in Fig. 3(b), 3(c) and 3(d) will be called Frame "a," Frame "b," and Frame "c," respectively, throughout this paper.

The total gravity loads per floor are equal for all three prototypes. The dead loads include the concrete floor slab, steel floor deck, mechanical equipment, floor and ceiling finishes, cladding weight, and an estimated weight per square

foot of structural steel. The seismic mass of each floor, excluding the roof level, included the dead load plus 0.72 kPa for partitions, as per ASCE7 [6]. The "tributary" seismic masses associated with the SC-CBF, from the first floor to the roof, are: 377000 kg, 375000 kg, 375000 kg, and 188000 kg. The initial PT bar stresses are assumed to be equal to 40% of the yield stress for all three frames.

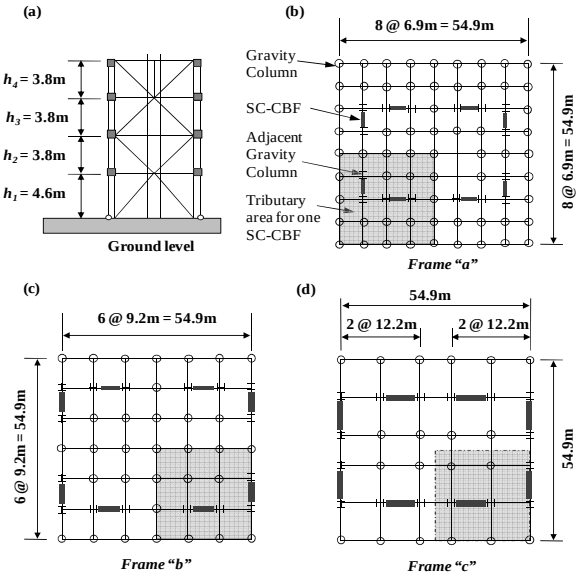

Fig. 3 Prototype structures: (a) typical elevation; (b) floor plan for Frame "a;" (c) floor plan for Frame "b;" (d) floor plan for Frame "c".

IV. Design Summary

The performance-based design procedure [5] for SC-CBF systems with friction-based energy dissipation is used in this study to design prototype SC-CBFs with different frame geometries.

TABLE I
FRAME PARAMETER COMPARISON

	Frame "a"	Frame "b"	Frame "c"
b_{bay} (m)	6.9	9.2	12.2
η	0.25	0.35	0.48
W (kN)	203.6	173.8	202.4
A_{PT} (mm^2)	10140	6120	4840
β_E	0.43	0.59	0.79
OM_D (MN-m)	14.1	13.8	19.4
OM_Y (MN-m)	34.1	32.9	45.2

Table I summarizes seven parameters of the SC-CBF designs: frame bay width (b_{bay}), design parameter η, total SC-CBF member weight (W), the area of the PT bars (A_{PT}), the hysteretic energy dissipation ratio (β_E), the overturning moment capacity at decompression (OM_D), and the overturning moment capacity at PT bar yielding (OM_Y). The member selections for the three designs are summarized in Table II.

Table I shows that Frame "c," which has the highest frame bay width, has the highest value of η; conversely, Frame "a," which has the lowest frame bay width, has the lowest value of η. As the value of η increases, the energy dissipation ratio β_E increases and the required PT bar area decreases. The member force design demands are highly dependent upon the PT bar yield force [5]; therefore, increasing η helps to reduce the sizes of the SC-CBF members. As the PT bar yield force is reduced (i.e., as A_{PT} decreases), the force demands in these members are reduced, and consequently the member sizes tend to be reduced, as shown in Table II. Though the member sizes decrease with increasing η, the weights of the structures do not follow the same trend due to the differing frame width (i.e., beam and brace length) of the three prototypes.

TABLE II
FRAME MEMBER SELECTION SUMMARY

		Frames		
	Story	"a"	"b"	"c"
Braces	1	W14x159	W14x109	W14x109
	2	W14x109	W14x90	W14x90
	3	W14x176	W14x132	W14x145
	4	W14x90	W14x74	W14x68
Beams	1[a]	W16x100	W16x100	W16x100
	2[a]	W16x77	W16x67	W16x67
	3[a]	W16x67	W16x67	W16x67
	4[a]	W16x89	W16x67	W16x67
Columns	1	W14x233	W14x159	W14x145
	2	W14x233	W14x159	W14x145
	3	W14x90	W14x68	W14x68
	4	W14x90	W14x68	W14x68
Strut	4	W14x211	W14x120	W14x99

[a] indicates floor levels for beams

V. Pushover Response

Pushover analyses of each frame were used to verify that the SC-CBFs exhibit the expected behavior and to compare their responses. The load profile used for each analysis is proportional to the first mode forces, calculated based on the elastic mode shapes of the fixed-base SC-CBF. The analyses were performed using the OpenSEES nonlinear analysis software [7]. The responses from monotonic pushover analyses of all three frames are shown in Fig. 4, which plots the applied overturning moment versus the roof drift.

The elastic stiffness of each frame is a function of the SC-CBF members; therefore, Frame "c" has a slightly greater elastic stiffness than the other frames. The limit state of column decompression is a function of the initial force in the PT bars, the weight of the SC-CBF members, and the frame width. As shown in Table I and Fig. 4, Frame "c" has the highest value of OM_D, whereas the values of OM_D for Frame "a" and Frame "b" are very close; the difference in initial PT bar forces and frame weights for Frames "a" and "b" are offset

by the difference in frame width. Note that the hysteresis loops in Fig. 5 show a reduction in slope before OM_D is reached; this is likely due to redistribution of the friction forces at the lateral-load bearings. As shown in Table I and Fig. 4, Frame "c" has the highest value of OM_Y and Frame "b" has the lowest. OM_Y is a function of PT bar area and frame width. The roof drift capacity at PT bar yielding, which is a function of initial PT bar stress and frame geometry, is the highest for Frame "a" and the lowest for Frame "c." Therefore, for these designs with identical initial stresses in the PT bars, the increase in frame width (increase in the value of η) results in a decrease in the roof drift capacity at PT bar yielding.

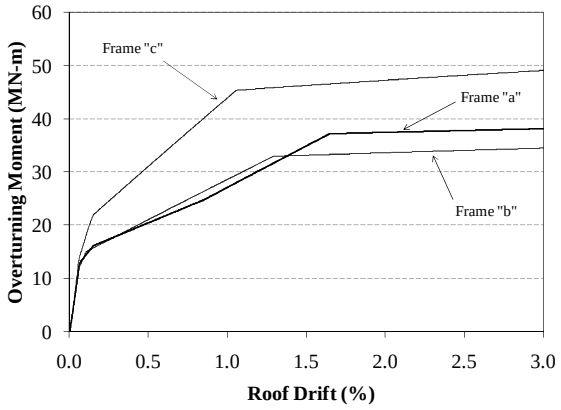

Fig. 4 Monotonic pushover response to PT bar yielding

The difference in energy dissipation ratio (β_E) for the three SC-CBF designs, as tabulated in Table 1, is evident in Fig. 5, which shows results from cyclic pushover analyses to 1% roof drift. Frame “c” has a relatively wide hysteresis loop with a high value of OM_D, and has the highest value of β_E. Frame "a" and Frame "b" have similar values of OM_D; however, the hysteresis loop for Frame "b" is wider than that of Frame "a;" therefore, β_E is greater for Frame "b" than for Frame "a."

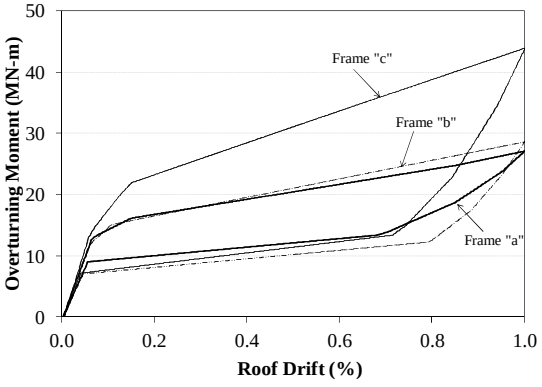

Fig. 5 Cyclic pushover response to 1% roof drift

VI. Seismic Response

A suite of 30 scaled DBE-level ground motions [5] was used to determine the seismic response of each frame. The beams, columns, and braces of the SC-CBF were modeled as linear elastic to permit the determination of the member force demands required to keep the members linear elastic. The PT bars were modeled using nonlinear beam-column elements with a post-yielding stiffness equal to 2% of their elastic stiffness. The gap opening behavior at the column bases was modeled using gap elements that resist compression but no tension. The friction behavior at the lateral load bearings was modeled using contact friction elements. Contact friction elements are gap elements that develop a friction force perpendicular to the applied compressive force. Rayleigh damping was used with 2% damping in the first mode and 5% in the third mode.

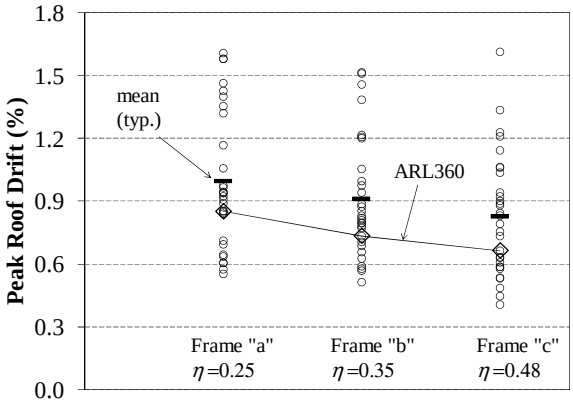

Fig. 6 Dynamic peak roof drift response for 30 DBE-level ground motions

Fig. 6 shows the peak roof drift response for each frame for the 30 DBE-level ground motions. The peak roof drift response tends to decrease with increasing η. The mean peak roof drift values are 0.99%, 0.91%, and 0.82% for Frames "a," "b," and "c," respectively. This trend in peak roof drift response is consistent with the effect of the increase in β_E shown in Table I.

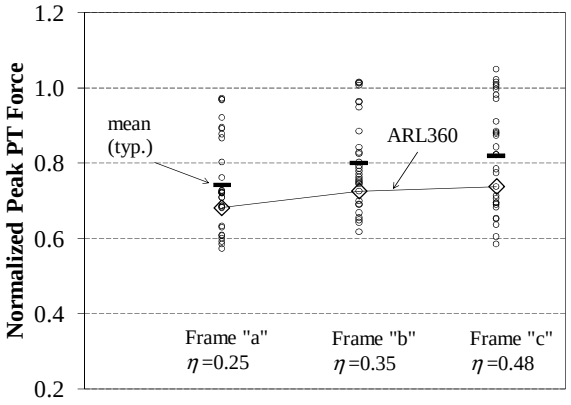

Fig. 7 Dynamic peak PT bar force response normalized by PT yield force for 30 DBE-level ground motions

Fig. 7 shows the peak PT bar force response normalized by

the PT bar yield force; as noted in Table I, each SC-CBF has a different PT bar area, leading to different PT bar yield forces. Normalized PT bar force values exceeding 1.0 indicate that PT bars yielded; the increased force response is due to strain hardening in the PT bars. The peak normalized PT bar force response for Frame "a" is less than 1.0 for each of the 30 ground motions. For Frame "b" and Frame "c", the peak normalized PT bar force response marginally exceeds 1.0 for several ground motions. In general, the peak normalized PT bar force response tends to increase slightly with increasing η. The average normalized peak PT bar force responses are 0.74, 0.80, and 0.82 for Frames "a," "b," and "c" respectively

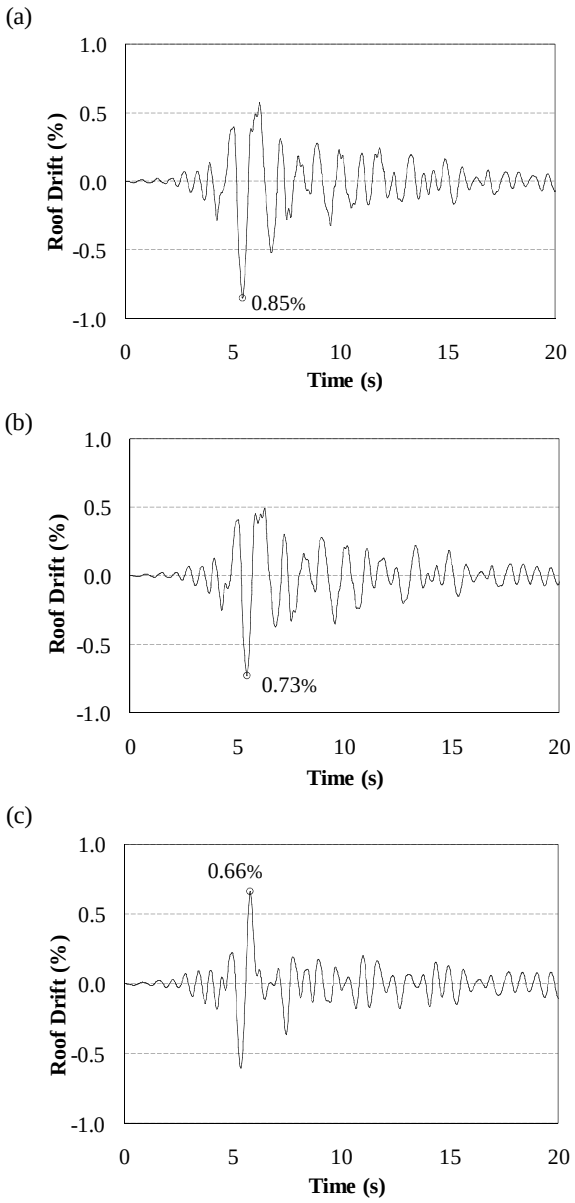

Fig. 8 Dynamic roof drift response to DBE_ARL360: (a) Frame "a"; (b) Frame "b"; (c) Frame "c".

The peak roof drift and normalized PT bar force responses to DBE_ARL360 are also indicated in Fig. 6 and Fig. 7. This record was chosen as representative of the SC-CBF behavior because the peak roof drift and normalized PT bar force responses for Frames "a," "b," and "c" follow the trends of the mean values.

The dynamic roof drift response of each frame to DBE_ARL360 is shown for each frame in Fig. 8. The peak roof drift responses to DBE_ARL360 are 0.85%, 0.73%, and 0.66%, for Frames "a," "b," and "c" respectively, following the trend of the mean values for the frames (i.e., decreasing peak roof drift response with increasing η).

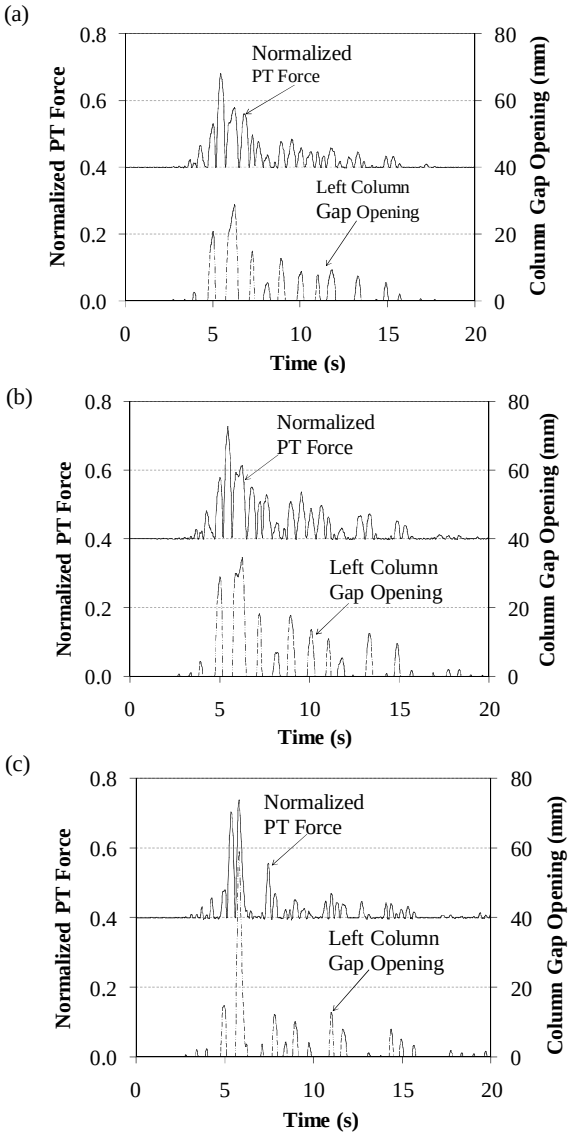

Fig. 9 Dynamic PT bar force normalized by PT yield force and column gap opening response to DBE_ARL360: (a) Frame "a;" (b) Frame "b;" (c) Frame "c."

Fig. 9 shows the dynamic PT bar force and column base gap opening response of each frame to DBE_ARL360. For simplicity, only the column base gap opening at the left SC-CBF column is shown. Following the expected behavior of

SC-CBF systems, the PT bar force is at its maximum when the column base gap opening is at its maximum. These points also correspond to the times of maximum roof drift (see Fig. 8). The magnitude of the column gap opening is higher for Frame "c," but the maximum normalized PT bar force is not significantly affected by η, increasing only slightly with increasing η.

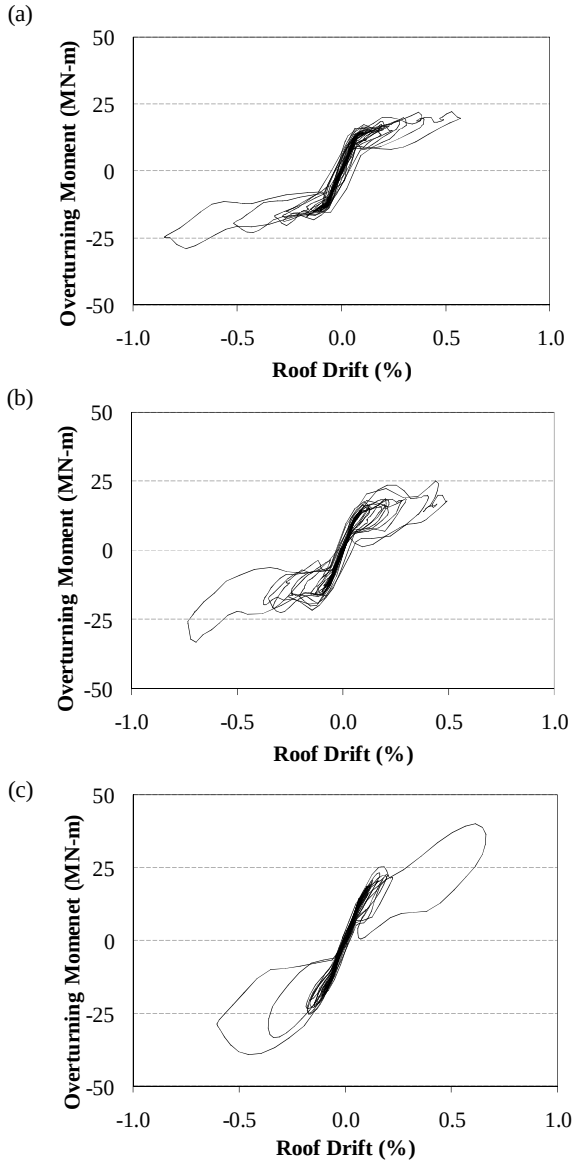

Fig. 10 Dynamic overturning moment versus roof drift hysteretic response to DBE_ARL360: (a) Frame "a;" (b) Frame "b;" (c) Frame "c."

Fig. 10 shows the overturning moment-roof drift hysteretic response of each frame to DBE_ARL360. Each frame exhibits the flag-shaped hysteresis loops that are characteristic of SC systems. The deviation from consistent bilinear behavior is likely due to higher mode effects on overturning moment after rocking [5].

VII. Summary And Conclusion

This paper describes a study of SC-CBF systems with friction-based energy dissipation and varied frame geometry. Three different prototype frames were considered in this study. Nonlinear static and dynamic analyses were performed to determine the effect of changing the frame geometry (thereby changing the design parameter η) on the behavior of the SC-CBF system.Design comparisons show that increasing the value of η tends to reduce the member sizes and the area of PT steel, while increasing the energy dissipation ratio β_E. The total weight of the SC-CBF is a function of PT bar area, frame member sizes, and the SC-CBF bay width; therefore, there is no simple relationship between η and the weight of the structural members.Static analysis results show that the overturning moment capacities at decompression and PT bar yielding are not exclusively functions of η, but are also dependent upon the weight of the structure and the PT bar area. Dynamic analysis results indicate that increasing the frame width (increasing the value of η) tends to decrease the peak roof drift response, which is consistent with the effect of the increase in energy dissipation ratio. The probability of the SC-CBF system reaching the PT bar yielding limit state under DBE level ground motions tends to increase slightly with the increase in the value of η; however, the probability of PT bar yielding is in accordance with the SC-CBF performance-based design criteria.

References

[1] Fahnestock, L.A.; Sause, R.; &Ricles, J.M. (2007a). “Seismic Response and Performance of Buckling-Restrained Braced Frames,” ASCE Journal of Structural Engineering 133(9): 1195-1204.

[2] Fahnestock, L.A.; Sause, R.; &Ricles, J.M. (2007b). “Experimental Evaluation of a Large-Scale Buckling-Restrained Braced Frame,” ASCE Journal of Structural Engineering 133(9): 1205-1214.

[3] Roke, D; Sause, R.; Ricles, J.M.; Seo, C.-Y.; & Lee, K.S. (2006). “Self-Centering Sesimic-Resistant Steel Concentrically-Braced Frames,” Proceedings of the 8th U.S. National Conference on Earthquake Engineering, EERI, San Francisco, USA.

[4] Roke, D; Sause, R.; Ricles, J.M.; & Chancellor, N.B. (2008). “Design Concepts for Damage-Free Sesimic-Resistant Self-Centering Steel Concentrically-Braced Frames,” Proceedings of the 14th World Conference on Earthquake Engineering, Beijing, China.

[5] Roke, D.; Sause, R.; Ricles, J.M.; & Chancellor, N.B. (2010). “Damage-Free Seismic-Resistant Self-Centering Concentrically-Braced Frames.” ATLSS Report 10-09, Lehigh University, Bethlehem, PA, USA.

[6] ASCE (2010).Minimum Design Loads for Buildings and Other Structures, ASCE7-10.American Society of Civil Engineers, Reston, VA, USA.

[7] Mazzoni, S.; McKenna, F.; Scott, M.H.; Fenves, G.L.; et al. (2009).Open System for Earthquake Engineering Simulation (OpenSEES) User Command-Language Manual. Pacific Earthquake Engineering Research Center, University of California, Berkeley.